



PAPER • OPEN ACCESS

Fabrication of bulk heterojunction organic solar cells with different configurations using electrospray

To cite this article: S K Shah 2020 *Nano Ex.* 1 020037

View the [article online](#) for updates and enhancements.

You may also like

- [Investigation of improvement in stability and power conversion efficiency of organic solar cells fabricated by incorporating carbon nanostructures in device architecture](#)

B V R S Subramanyam, Prakash Chandra Mahakul, Kadambinee Sa et al.

- [Revisiting open-circuit photovoltage decay in organic solar cells for the determination of bimolecular recombination constants](#)

Emi Nakatsuka, Kiyohito Mori, Naoki Ueno et al.

- [Efficient charge generation at low energy losses in organic solar cells: a key issues review](#)

Ye Xu, Huifeng Yao, Lijiao Ma et al.

ECS
The
Electrochemical
Society
Advancing solid state &
electrochemical science & technology

DISCOVER
how sustainability
intersects with
electrochemistry & solid
state science research



PAPER

Fabrication of bulk heterojunction organic solar cells with different configurations using electrospray

OPEN ACCESS

RECEIVED
9 July 2020ACCEPTED FOR PUBLICATION
15 July 2020PUBLISHED
11 September 2020

Original content from this work may be used under the terms of the [Creative Commons Attribution 4.0 licence](#).

Any further distribution of this work must maintain attribution to the author(s) and the title of the work, journal citation and DOI.



S K Shah

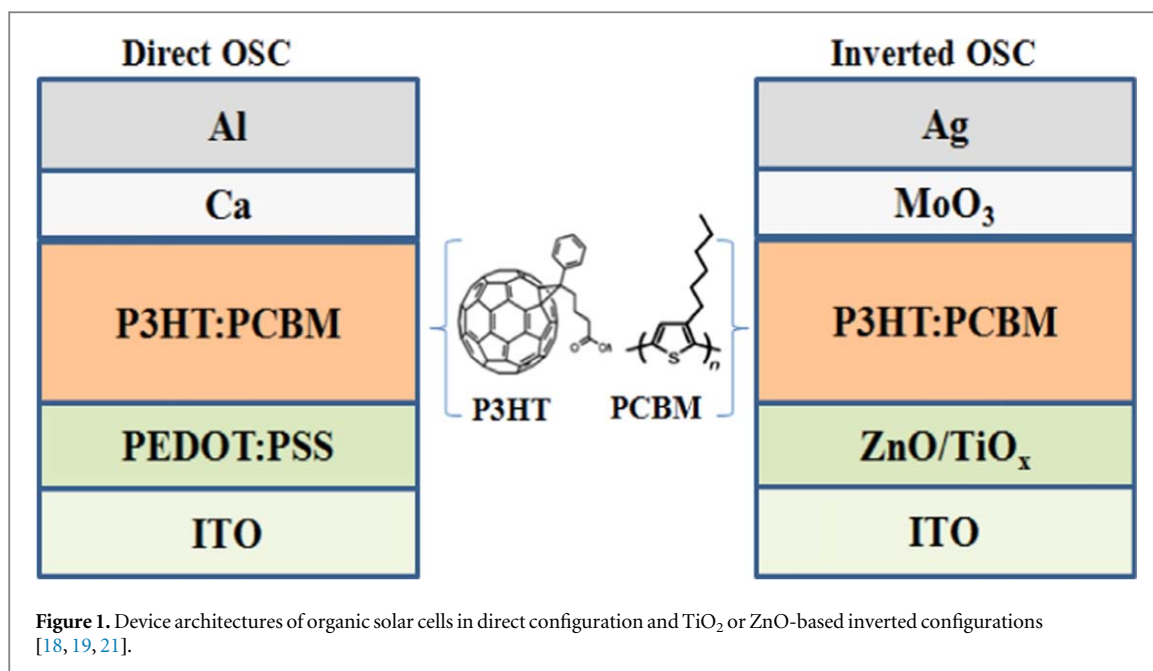
Department of Physics, Abdul Wali Khan University Mardan, Khyber Pukhtunkhwa, 23200, Pakistan

E-mail: saidkarim@awkum.edu.pk**Keywords:** bulk heterojunction organic solar cells, electrospray deposition, direct structure OSC, ZnO/TiO₂ based inverted OSCs, J-V characteristics**Abstract**

In this work, we fabricated bulk heterojunction (BHJ) organic solar cells (OSCs) using electrospray deposition (ESD) with two different device configurations. ITO/PEDOT:PSS/P3HT:PCBM/Ca/Al and ITO/ZnO and TiO₂/P3HT:PCBM/MoO₃/Ag, termed as direct and inverted OSCs, respectively. In ZnO/TiO₂-based inverted solar cells, ZnO/TiO₂ films were synthesized by sol-gel process and deposited on ITO deposited glass substrates using the spin-coating technique. P3HT/PCBM blend layers were deposited by using electrospray deposition (ESD). To observe the thermal effects on the device efficiencies, the devices were annealed at different temperatures (up to 140 °C). The cell's performance parameters were compared at an annealing temperature of 120 °C. Comparing the performance parameters of both types of OSCs at an annealing temperature of 120 °C, the power conversion efficiency (PCE) the 1.62% is found for direct-structured OSC while 1.57% and 1.0% for ZnO/TiO₂-based inverted structures, respectively. Interestingly, the enhanced device performance parameters were obtained with oxides-based OSCs. Compared to ZnO-based inverted OSC, the TiO₂-based inverted OSC has lower efficiency which might be due to the highly resistive surface of TiO₂ with deep-level traps. These traps can be reduced by light soaking to achieve the optimal power conversion efficiency.

1. Introduction

Photovoltaic (PV) technology is still in an exciting phase with rapid improvements in terms of materials selection, device engineering and fabrication techniques. In the last two decades, bulk heterojunction (BHJ) organic solar cells (OSCs) have drawn considerable attention of many research groups due to their excellent optical and electrical properties. OSCs offer multiple advantages over the conventional technology for being solution-based, working at lower temperature and have lower production costs [1]. Apart from their application in PV, organic solar cells have the potential of having conjugated polymers for low-cost fabrication of large-area integrated devices on both rigid and flexible substrates [2, 3]. The efficiency of P3HT/PCBM based OSCs have already been reported up to 5% [4, 5] and since then was variously designed to exceed 10% using special low bandgap materials [6] and by sophisticated device geometries. Generally, the OSC device's performance in bilayer configuration, is limited by poor excitons dissociation at donor(D)/acceptor(A) interface due to the diffusion length of the excitons in organic materials, charge carrier transport, high rates of excitons recombination and low charge carrier motilities of organic semiconductor materials. Therefore, in the bulk heterojunction OSC, the intimate mixing of the donor (D) and acceptor (A) materials, the charge transfer at D/A interface increases. When light falls on the OSCs, excitons are created and start diffusing towards D/A interface for charge generation to occur. Therefore, efficient charge generation requires that each exciton has to find a D/A interface within a diffusion length of the excitons of organic materials (around 5 to 10 nm), otherwise, excitons will be lost without charge generation and separation. An intimate bi-continuous interpenetrating network of D/A materials in the nanometer range should suppress excitons loss before charge generation.



Therefore, an efficient charge generation at D/A interface and suppression of excitons loss requires control over the morphology of photoactive films providing percolation pathways for charge carriers transport towards their respective electrodes. The common architecture of bulk heterojunction organic solar cells (OSCs) in the direct configuration, the blend solution from P3HT, donor material and PCBM, acceptor material is deposited on PEDOT:PSS/ITO substrates, using electro spray deposition followed by Ca/Al [7] deposition by thermal evaporation, this structure of the device is shown in figure 1. On the other hand, P3HT/PCBM blends layer is sandwiched between the transition metal oxide layers such as ZnO and TiO₂ (on ITO substrates), are used as electron-extracting electrodes [8–12] and high work function metals, such as gold or silver (Au or Ag) with MoO₃ [13, 14] or V₂O₃ [15], used as hole-collecting electrodes, such configurations of the devices are known as inverted OSCs. At variance with direct conventional architecture [16, 17], where ITO is a hole collector, the photo-generated charge carriers flow through the external circuit from the transparent electrode indium tin oxide (ITO) to the hole collecting MoO₃/Ag [14] contact. The metals oxides ZnO/TiO₂ layers were used as the electron transporting layers and were deposited by spin coating from the sol-gel processes [18, 19]. Due to high transparency in the visible and near-infrared, ZnO/TiO₂ can be used as interface modification at the ITO surface in the inverted structure of OPV devices. In this study, we have employed electro spray deposition (ESD) that is an alternative approach for organic solar cells fabrication for layer by layer deposition of thin films. Electro spray deposition (ESD) has a unique advantage, as compared to other deposition techniques, where an ultra diluted solution is used to separate solvent and solute in a quite efficient way [20]. This is a very important aspect of utilizing, ESD for a wide range of low solubility materials in device applications [21, 22–25]. It is also a very promising technique for fabricating high-performance OSCs at low processing temperature [25–27]. The main advantages of using our homemade ESD system for active layer deposition of OSCs over the other deposition techniques is that the growth rate of the film is relatively high, efficient usage of materials and uniform distribution over the entire surface. This process can be carried out in a vacuum or an ambient condition in a controlled manner. Moreover, layer by layer deposition of thin films with double-solvent/solute approach makes electro spray deposition a better choice for fabricating OSCs [21, 23, 24]. Here, we report bulk heterojunction organic solar cells in both direct and inverted configuration using ESD. Secondly, the device performance parameters of the fabricated devices such as short circuit current density (J_{SC}), open-circuit voltage (V_{OC}), fill factor (FF) and power conversion efficiency (PCE) are compared as a function of varying annealing temperature. Interestingly, OSCs have shown similar trends to those reported in our earlier studies [21, 23, 24]. After thermal annealing at 120 °C, OSCs exhibit the power conversion efficiencies (PCEs) of 1.62% in a direct structure, 1.57% in ZnO -based inverted structure and 1.0% in TiO₂ -based inverted OSC. The poor performance of the TiO₂ -based device is probably due to some defect states present in the TiO₂ surface which may be reduced by light soaking before testing the cell. Poor diode behaviour and bad rectification may also be the reason for the lower efficiency of TiO₂ -based device.

2. Experimental methods and materials

Transparent conducting oxide (TCO) coated glass substrates such as indium tin oxide (ITOs) were used as working electrodes. ITOs were cleaned in an ultrasonic bath by using standard procedures [21] and treated with UV-Ozone for 10 min. For device fabrication: (1) For direct structure devices, the transparent hole conducting polymer film around 30 nm, poly(3,4-ethylenedioxythiophene):polystyrene sulfonate (PEDOT:PSS) (Aldrich) was spin-coated on ITO/glass substrates at 4000 rpm for the 40 s. The films were, then, annealed at 110 °C for 30 min in a vacuum oven. P3HT/PCBM blend active layers, with 0.5 mg ml⁻¹ of solution concentration, was deposited on PEDOT:PSS coated ITO substrate by ESD with a flow rate of 1.3 μl s⁻¹ where the applied voltage was 2kV. A 100 nm aluminium (Al) was thermally deposited as a top counter electrode with an operating pressure of 1.33 × 10⁻⁷ kPa onto the active layer to complete the direct OSC structure. (2) For inverted structured devices, ZnO and TiO₂, layers were processed using the sol-gel method at low temperature, while for the electron transport/hole blocking layers on ITO/glass substrates, the synthesis processes detailed in our previous studies were followed [21, 26]. The active layers of P3HT/PCBM blends were deposited by ESD onto the ZnO/TiO₂ coated ITO substrates following the same deposition parameters as described for the direct OSC [18, 19, 21, 12–17, 20, 22–26]. To complete the device structure, a 6 nm of MoO₃ as a hole extraction layer, followed by 60 nm of Ag, were deposited by thermal evaporation at a base pressure of 1.33 × 10⁻⁷ kPa through shadow mask of cell active area of 8.6 mm². The surface morphology of samples were investigated with atomic force microscope (AFM) using digital instruments dimension of 3100 in tapping mode and quantitative morphological analysis was performed using the WSxM software. Ultraviolet-visible (UV-vis) absorption of the films was carried out at a scan range of 300–800 nm using Perkin Elmer 19 spectrometer. Current-voltage (J-V) characteristics of the devices were examined under an inert atmosphere using a Keithley 4200 semiconductor analyzer under the illumination of an AM1.5 set at 100 mW cm⁻² calibrated by an IL1400BL radiometer.

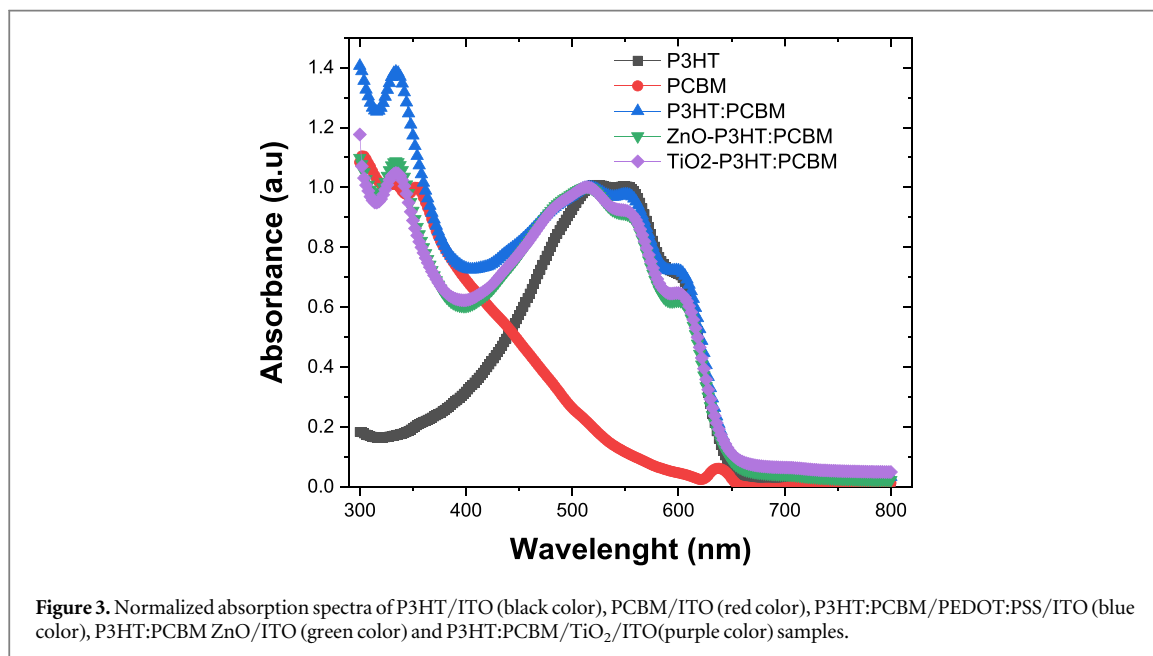
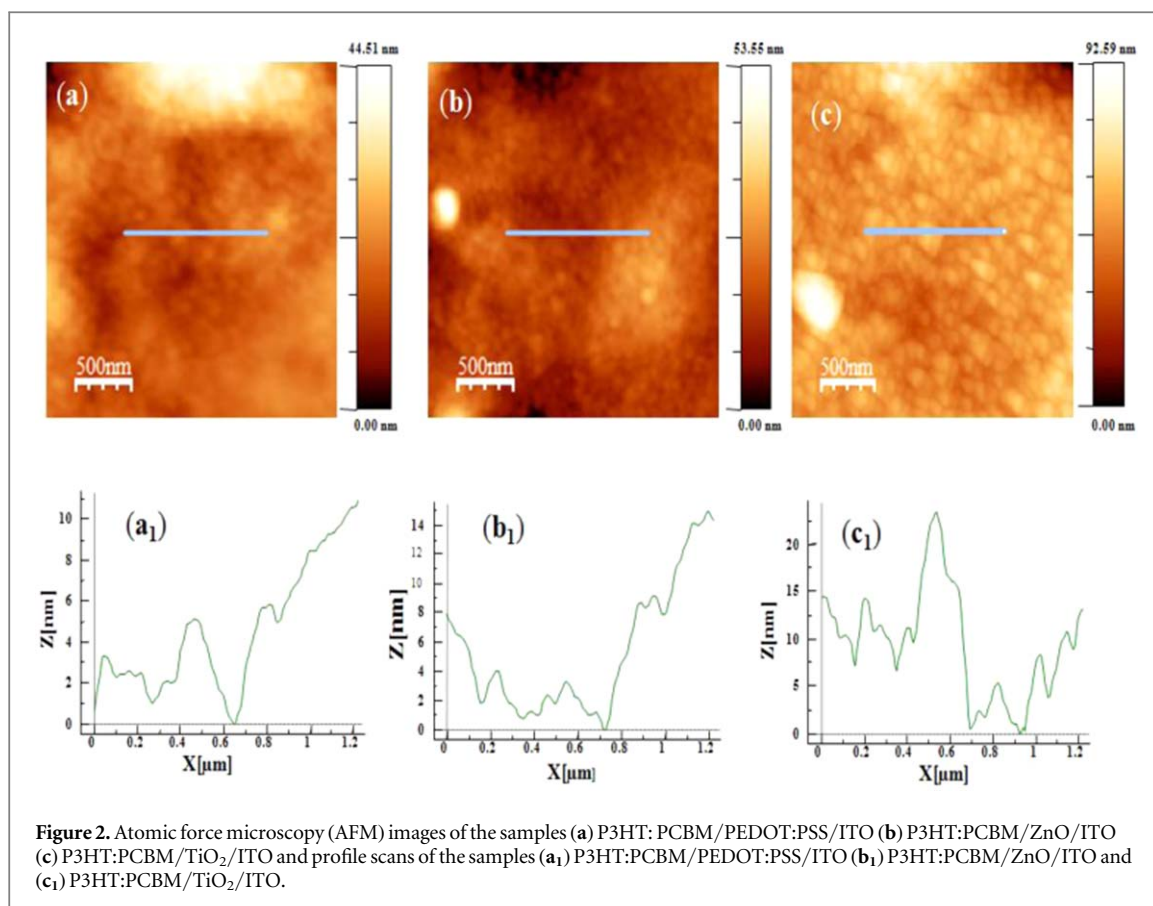
3. Results and discussions

Figure 1 describes the configuration of the device which consists of P3HT and PCBM as active materials, deposited on PEDOT:PSS coated ITO substrate followed by the metallization of Ca/Al (direct-structured OSC) and MoO₃/Ag (inverted- structured OSCs) as the top counter electrode. In OSC devices, the photo-generated carriers, holes and electrons must be able to move to the corresponding electrodes through materials intimately mixed P3HT/PCBM. The holes are transported by the P3HT (donor) to one electrode and electrons by the PCBM (acceptor) material to the next electrode on the other side of the devices depending on the structure of the device. The photoactive materials such as P3HT and PCBM are mixed in the form of blend film to provide a bi-continuous interpenetrating network in which cul-de-sacs or barriers are avoided.

Figure 2 shows the atomic force microscopy (AFM) topography of P3HT-PCBM blend on PEDOT:PSS coated ITO substrate (figure 2(a)) and on ZnO/TiO₂ coated ITO substrates [figures 2 (b) and (c)]. The profile scans of the AFM images show the particles in the range of 100 nm at the nano-scale morphology. The root mean square (RMS) roughness of P3HT-PCBM blend on PEDOT:PSS-coated ITO substrate is 3 nm and ZnO and TiO₂-coated ITO substrates are 4 nm and 7 nm, respectively. The surface phase separation of P3HT and PCBM is more evident in the case of TiO₂, forming a rougher surface of the film.

Figure 3 shows the UV-vis spectra of P3HT, PCBM, P3HT:PCBM, ZnO/P3HT:PCBM and TiO₂/P3HT:PCBM films. Generally, P3HT/PCBM blend films exhibit strong absorption in the visible region from 300 nm to 750 nm. The absorption spectra of ZnO/P3HT:PCBM and TiO₂/P3HT:PCBM films closely resemble with each other, while in case of P3HT:PCBM film the excess photon absorption is seen at a wavelength around 330 to 400 nm. A strong absorption was observed in the visible region with intense peaks occurred at around 330 nm and 550 nm and corresponds to electronic transition $\pi-\pi^*$, of P3HT while associated with the formation of excitons with phonons [28]. The PCBM film shows absorption in the range around 330 to 450 nm. There is a sharp shoulder peak, around 600 nm in the absorption spectra corresponding to vibronic features, suggesting a more organized and well-ordered structure of the polymer backbone within the matrix [5, 29].

Figure 4 presents the J-V characteristics of ESD devices which were tested under the solar simulator of the light intensity at AM1.5 G (100 mW cm⁻²). The efficiency of direct-structured OSCs of 1.78% (at 110 °C) is higher than that of inverted OSCs. It is due to higher conductivity and higher surface quality of PEDOT:PSS as a hole transport layer in direct OSCs, than in ZnO/TiO₂ as electron transport layers in the inverted OSCs. However, at thermal annealing of 120 °C, the direct-structured cell exhibited an efficiency of 1.62% while the inverted OSCs exhibited efficiencies of 1.57% (ZnO) and 1.0% (TiO₂). The performance parameters of the devices are shown in table 1. The series resistance of the OSCs was observed to be 21 Ω (direct), 28 Ω (ZnO inverted) and 88 Ω (TiO₂ inverted). TiO₂ based OSC with a poor FF of 36% and shows an inflexion point in the



JV-curve with a kink in the curve can be seen in the fourth quadrant. It might be due to the fact that the TiO₂ based devices require light activation mechanism as the as-deposited TiO₂ films are highly resistive due to the presence of defect states (oxygen vacancies), which can be significantly reduced by light soaking before testing the cell. It may also be due to the surface roughness of TiO₂/P3HT:PCBM film and a series resistance of the device. Most importantly, the trend of ESD devices is consistent with that reported in our previous studies [21, 23, 24]. Compared to TiO₂ based inverted OSC, direct as well as ZnO-based inverted structured devices, show better diode behaviour with higher rectification as shown in figure 4(b).

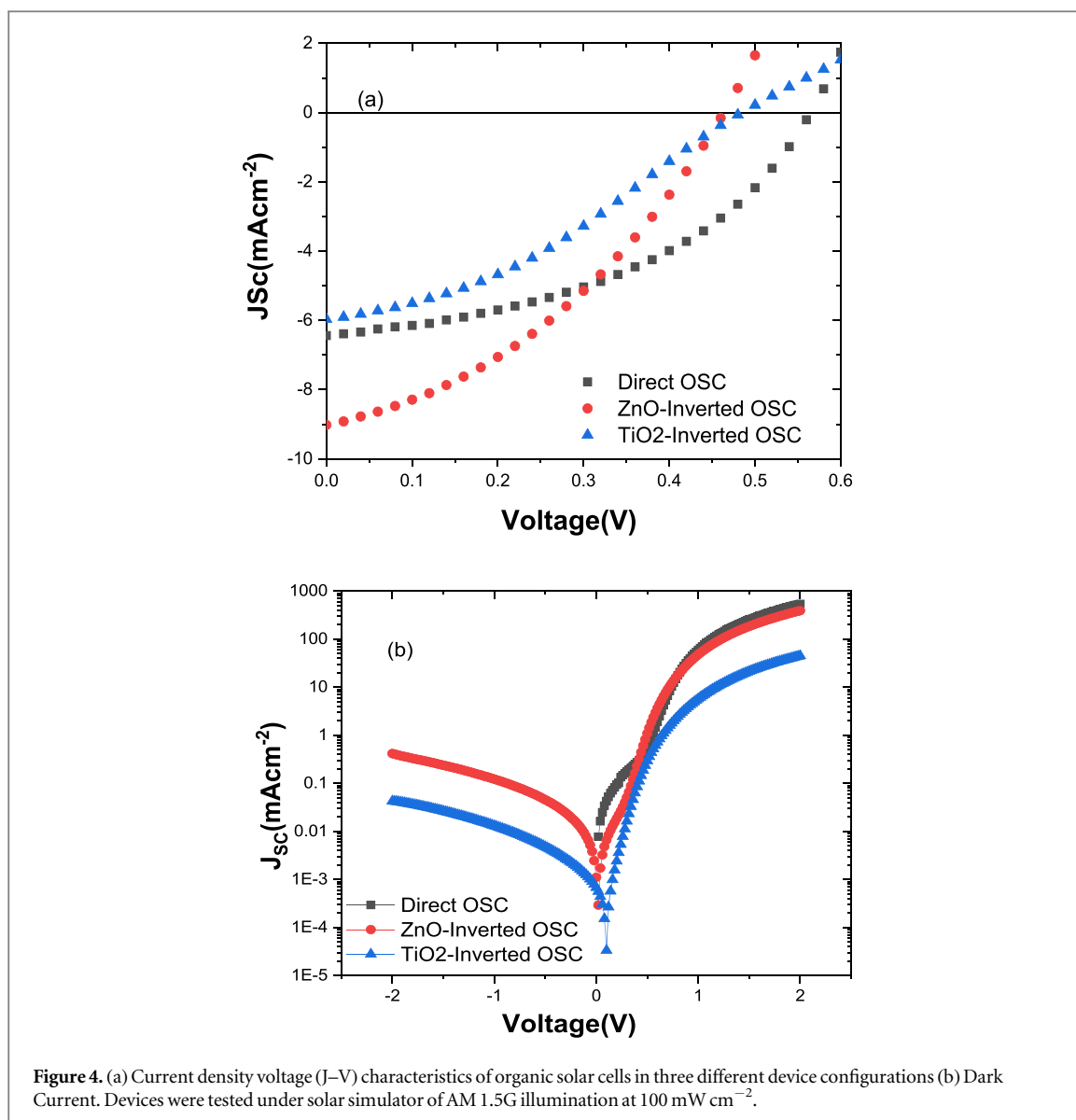
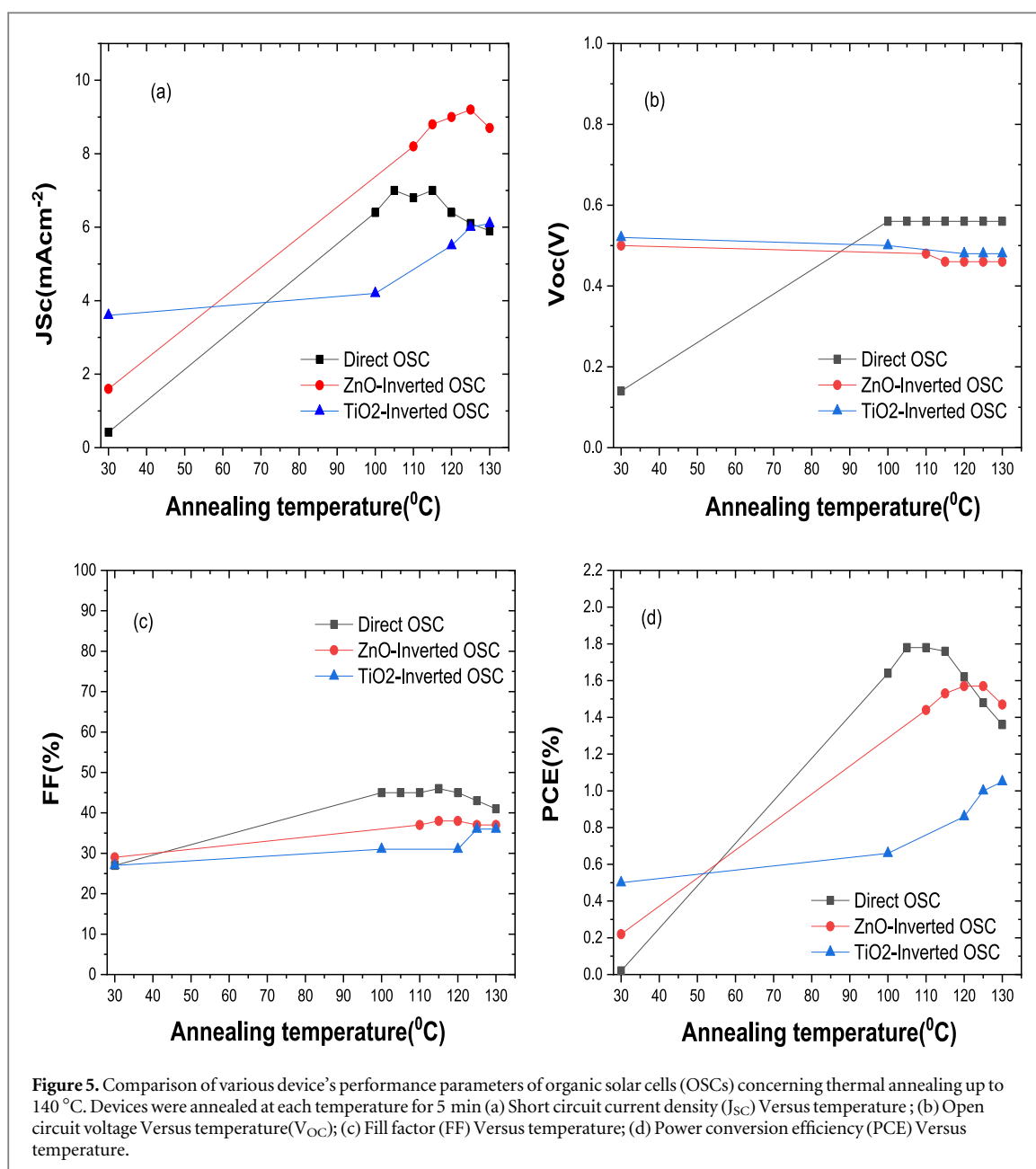


Figure 4. (a) Current density voltage ($J-V$) characteristics of organic solar cells in three different device configurations (b) Dark Current. Devices were tested under solar simulator of AM 1.5G illumination at 100 mW cm^{-2} .

Table 1. Devices' performance parameters of organic solar cells at an annealing temperature of 120°C in direct and ZnO/TiO₂-based inverted configurations. Devices were tested under solar simulator of AM 1.5G illumination at 100 mW cm^{-2} .

Devices/ Parameters	J_{SC} (mAcm^{-2})	V_{OC} (V)	FF (%)	PCE (%)
Direct OSC	6.4	0.56	45	1.62
ZnO Inverted OSC	9	0.46	38	1.57
TiO ₂ Inverted OSC	6	0.48	36	1.0

The devices' performance parameters of OSCs such as J_{SC} (short circuit current density), V_{OC} (open circuit voltage), FF (fill factor) and the PCE (power conversion efficiency), were studied as a function of annealing temperature as shown in figure 5. The device's performance parameters increase with increasing annealing temperature of the devices. The variation in the device efficiency is mainly followed by the changing trend in the device's performance parameters for an instance, J_{SC} , V_{OC} and FF in figures 5(a), (b) and (c) respectively. J_{SC} depends on the photon to current conversion processes, starting from photon absorption to the charge carrier transport to the corresponding electrodes. Whereas, V_{OC} mainly depends on the intensity of light, thermal annealing, materials structure and the work function of the electrodes [30]. The fill factor (FF) determines the



maximum power of the solar cells is related to J_{SC} and V_{OC} . Compared to the V_{OC} and J_{SC} , FF is a more sensitive parameter of solar cell which depends on thickness, mobility and lifetime of the product of the active materials and the interface between electrodes to active layer materials [31]. Based on these mentioned terms, FF is influenced by, the charge carrier recombination losses, decreasing the series resistance, increasing the shunt resistance and decreasing the reverse saturation current (I_s). The decreasing in the efficiency of OSCs with increasing temperature above 120 °C is due to some degradation mechanisms, present in the devices with ESD deposition process [22]. As the ESD films after deposition were exposed to air for a couple of weeks before contact metallization, causing oxidization of the film [32]. Therefore, at higher annealing temperatures, the top electrode (Al) got oxidized, and in parallel R_s of the device increased, due to the Al₂O₃ layer between the active layer and metal electrodes. However, the saturation of V_{OC} in ESD devices are at rather low temperatures, confirming the well-ordered structure of P3HT molecules within the active layer blend films. It may be noted that V_{OC} is not affected by the change in the series resistance following the temperature treatment, as there is no current in open circuit condition. However, at higher annealing temperatures, the series resistance of ESD devices increases which affects the J_{SC} and FF of the devices leading to the deterioration of the device performance as shown in figures 5(a) and (c). In the inverted devices the PCEs suffer mostly by loss in V_{OC} and FF [21], 0.46, 38% (TiO₂-inverted) and 0.48, 36% (ZnO-inverted), as shown in figure 4(a). This is related to the interface between the active layer and electrode and probably the rich P3HT molecules at the interface, influencing electron extraction from PCBM to the oxide layer, thus diminishing the fill factor.

4. Conclusions

In summary, electrospray deposition (ESD) was used for the fabrication of bulk heterojunction organic solar cells (OSCs) in two different configurations, ITO/PEDOT:PSS/P3HT:PCBM/Ca/Al (direct structure) and ITO/ZnO and TiO₂/P3HT:PCBM/MoO₃/Ag (inverted structures). Device performance parameters of the OSCs were compared as a function of varying annealing temperature. It was observed that the ESD direct structured devices perform better than the inverted-structure devices. The efficiency of direct-structure OSCs of 1.78% (at 110 °C) is higher than those of inverted OSCs, which is due to higher conductivity and higher surface quality of PEDOT:PSS as a hole transport layer and lower series resistance (21 Ω) as compared to the surface quality of ZnO/TiO₂ as electron transport and higher series resistances of 28 Ω (ZnO-inverted) and 88 Ω (TiO₂-inverted) devices. However, at an annealing temperature of 120 °C, the device's performance parameters were compared and higher power conversion efficiency (PCE) of 1.62% was obtained for the direct-structured OSC while in case of ZnO/TiO₂-based inverted structures, the obtained PCEs are 1.57% and 1.0% respectively. The lower efficiency in case of TiO₂ based device is due to the surface defect which is highly resistive to as prepared OSC to activate. Hence, OSC with a poor FF shows an inflexion point in the JV-curve and a kink appears. It suggests that such devices need to have light soaking to give its optimal efficiency. In the inverted OSCs the loss in V_{OC} and FF (0.46, 38%) in TiO₂-based and (0.48, 36%) in ZnO-based OSCs is related to the interface between active layer and electrode. Besides, the low FF is due to the rich P3HT molecules at the interface, influencing electron extraction from PCBM to oxide layers. Interestingly, the trend of the device in terms of even better device performance parameters is quite consistent with previous work reported for ESD single-layer devices.

ORCID iDs

S K Shah  <https://orcid.org/0000-0003-0942-2464>

References

- [1] Krebs F C 2009 Fabrication and processing of polymer solar cells: are view of printing and coating techniques *Sol. Energy Mater. Sol. Cells* **93** 394
- [2] Güne S, Neugebauer H and Sariciftci N S 2007 Conjugated polymer-based organic solar cells *Chem. Rev.* **107** 1324–38
- [3] Chen J and Cao Y 2009 Development of novel conjugated donor polymers for high-efficiency bulk-heterojunction photovoltaic devices *Acc. Chem. Res.* **42** 1709–18
- [4] Li G, Shrotriya V, Huang J, Yao Y, Moriarty T, Emery K and Yang Y 2005 High-efficiency solution processable polymer photovoltaic cells by self-organization of polymer blends *Nat. Mater.* **4** 864
- [5] Reyes-Reyes M, Kim K and Carroll D L 2005 High-efficiency photovoltaic devices based on annealed poly(3-hexylthiophene) and 1-(3-methoxycarbonyl)-propyl-1-phenyl-(6,6)C₆₁ blends *Appl. Phys. Lett.* **87** 083506
- [6] Zhao J, Li Y, Yang G, Jiang K, Lin H, Ade H, Ma W and Yan H 2016 Efficient organic solar cells processed from hydrocarbon solvents *Nat. Energy* **1** 15027
- [7] Dang M T, Hirsch L and Wantz G 2011 P3HT:PCBM, best seller in polymer photovoltaic research *Adv. Mater.* **23** 3597
- [8] Sahin Y, Alem S, de Bettignies R and Nunzi J-M 2005 Development of air stable polymer solar cells using an inverted gold on top anode structure *Thin Solid Films* **476** 340
- [9] Waldauf C, Morana M, Denk P, Schilinsky P, Coakley K, Choulis S A and Brabec C J 2006 Highly efficient inverted organic photovoltaics using solution based titanium oxide as electron selective contact *Appl. Phys. Lett.* **89** 233517
- [10] White M S, Olson D C, Shaheen S E, Kopidakis N and Ginley D S 2006 Inverted bulk-heterojunction organic photovoltaic device using a solution derived ZnO underlayer *Appl. Phys. Lett.* **89** 143517
- [11] Li G, Chu C-W, Shrotriya V, Huang J and Yang Y 2006 Efficient inverted polymer solar cells *Appl. Phys. Lett.* **88** 253503
- [12] Shah S K and Gunnella R 2020 Efficient method of fabricating polymeric solar cells in multilayered configuration using electrospray *J. Elect. Mater.* **49** 1794–800
- [13] Kyaw A K, Sun X W, Jiang C Y, Zhao D W, Lo G Q and Kwong D L 2008 An inverted organic solar cell employing a sol-gel derived ZnO electron selective layer and thermal evaporated MoO₃ hole selective layer *Appl. Phys. Lett.* **93** 221107
- [14] Kolb F, Busby Y, Houssiau L and List-Kratochvil E J W 2019 In-depth investigation of the charge extraction efficiency for thermally annealed inverted bulk-heterojunction solar cells *J. Appl. Phys.* **125** 034502
- [15] Huang J S, Chou C Y and Lin C F 2010 Enhancing performance of organic/inorganic hybrid solar cells using a fullerene interlayer from all-solution processing *Sol. Energy Mater. Sol. Cells* **94** 182
- [16] Busby Y, List-Kratochvil E J W and Pireaux J-J 2017 Chemical analysis of the interface in bulk-heterojunction solar cells by x-ray photoelectron spectroscopy depth profiling *ACS Appl. Mater. Interfaces* **9** 3842–8
- [17] Shah S K, Khan J, Ullah I and Khan Y 2017 Optimization of active layer thickness top electrode and annealing temperature *AIMS Mater. Sci.* **4** 789
- [18] Ullah I, Shah S K, Wali S, Khattak S A and Hayat K 2017 Enhanced efficiency of organic solar cells by using ZnO as an electron transport layer *Mater. Res. Express* **4** 125505
- [19] Shah S K, Hayat K and Ali K 2019 Effect of TiO₂ interlayer on the performance of inverted polymeric solar cells *Mater. Res. Express* **6** 065102
- [20] Jaworek A 2007 Electrospray droplet sources for thin film deposition *J. Mater. Sci.* **42** 266
- [21] Shah S K, Gunnella R, Hirsch L and Abbas M 2017 Stability enhancement of polymer solar cells in trilayer configuration *J. Thin Solid Films* **640** 104

- [22] Ali M, Abbas M, Shah S K, Bontempi E, Colombi P, Di Cicco A and Gunnella R 2011 Variability of physical characteristics of electro-sprayed poly(3-hexylthiophene) thin films *Appl. Phys.* **110** 054515
- [23] Ali M, Abbas M, Shah S K, Tuerhong R J, Generosi A, Paci B, Hirsch L and Gunnella R 2012 Realization of solution processed multi-layer bulk heterojunction organic solar cells by electro-spray deposition *Org. Electr.* **13** 2130
- [24] Shah S K, Abbas M, Ali M, Hirsch L and Gunnella R 2014 Optimal construction parameters of electro-sprayed trilayer organic photovoltaic devices *J. Phys. D: Appl. Phys.* **47** 045106
- [25] Abbas M, Ali M, Shah S K, D'Amico F, Postorino P, Mangialardo S, Guidi M C, Cricenti A and Gunnella R 2011 Control of structural, electronic, and optical properties of eumelanin films by electro-spray deposition *J. Phys. Chem. B* **115** 11199
- [26] Shah S K, Ishaq M, Khattak S A, Ullah I, Hayat K, Khan M, Khan G and Tabbasam L 2019 Effect of Mesoporous TiO₂ thicknesses on the performance of solid-state dye-sensitized solar cells *J. Elect. Mater.* **48** 696–704
- [27] Ali M, Abbas M, Shah S K, Bontempi E, Di Cicco A and Gunnella R 2013 Film forming properties of electro-sprayed organic heterojunctions *Eur. Phys. J. Appl. Phys.* **62** 30202
- [28] Karagiannidis P G, Georgiou D, Pitsalidis C, Laskarakis A and Logothetidis S 2011 Evolution of vertical phase separation in P3HT:PCBM thin films induced by thermal annealing *Mater. Chem. Phys.* **129** 1207
- [29] Yao L G, Yang Y, Shrotriya H, Yang V and Yang G Y 2007 Solvent annealing $i_{1/2}$ effect in polymer solar cells based on poly(3-hexylthiophene) and Methanofullerenes *Adv. Funct. Mater.* **17** 1636
- [30] Qia B and Wang J 2012 Open-circuit voltage in organic solar cells *J. Mater. Chem.* **22** 24315–25
- [31] Gupta D, Mukhopadhyay S and Narayan K S 2010 Fill factor in organic solar cells *Sol. Energy Mater. Sol. Cells* **94** 1309–13
- [32] Hintz H, Egelhaaf H J, Ler L, Hauch J, Peisert H and Chass T 2011 Photodegradation of P3HT-A Systematic Study of Environmental Factors *Chem. Mater.* **23** 145